(Received 22 July 2025, Accepted 16 September 2025, Scheduled 19 February 2026)

Design of Directional Circularly-Polarized Dielectric Resonator Antenna with Different Radiating Angles

Qiheng Huang[1, 2, 3, 4] and Kwok Wa Leung[1, 2, 3, 4, *]

[1] *State Key Laboratory of Terahertz and Millimeter Waves and Department of Electrical Engineering City University of Hong Kong, Hong Kong, SAR, China*
[2] *City University of Hong Kong, Hong Kong, SAR, China*
[3] *Shenzhen Key Laboratory of Millimeter Wave and Wideband Wireless Communications CityU Shenzhen Research Institute, Shenzhen 518057, China*
[4] *Information and Communication Technology Centre, CityU Shenzhen Research Institute, Shenzhen 518057, China*

ABSTRACT: A directional circularly polarized dielectric resonator antenna for different main-beam angles is designed using the Particle Swarm Optimization (PSO) method. It is a single-feed, single-layer structure. For demonstration, the main-beam angle θ is designed at 30° and a 5G frequency of 5.8 GHz. To verify our design, a prototype is fabricated using 3D-printing technology. Its reflection coefficient, radiation pattern, realized gain, and the total antenna efficiency are measured. Measured results show good agreement with simulated ones. The prototype has a −10 dB impedance bandwidth of 37.24% (4.84–7 GHz), a 3-dB axial ratio bandwidth of 15.52% (5.3–6.2 GHz), a peak gain of 5.87 dBi, and a peak total antenna efficiency of 96%. It has a low profile of $0.2\lambda_0$, where λ_0 is the free-space wavelength at 5.8 GHz.

1. INTRODUCTION

Dielectric resonator (DR) antenna (DRA) has received much attention over the past decades since the seminal work by Long et al. [1]. Its inherent advantages, including compact size, high radiation efficiency, wide bandwidth, and ease of excitation, make it a strong candidate for 5G communication systems [2–5]. As a three-dimensional structure, DRA offers greater design flexibility than one- or two-dimensional antennas. This flexibility has led to numerous geometric innovations aimed at enhancing antenna performance.

Compared with linearly polarized (LP) antennas, circularly polarized (CP) antennas provide better signal stability and reduce multi-path interference [5]. In general, CP DRA designs [6–14] can be divided into two categories: multi- and single-feed configurations. Multi-feed techniques typically achieve wider axial ratio (AR) bandwidths, but require external hybrid couplers or power dividers, increasing system complexity, size, and insertion loss. In contrast, single-feed approaches (achieved by modifying the DR shape, adjusting the feeding structure, or introducing parasitic elements) offer simpler, more compact designs with lower loss, although the AR bandwidth is usually less than 10%. Various strategies have been proposed to overcome this limitation. They include the use of multiple DRs [13], excitation of higher-order modes [7], application of traveling-wave excitation sources [8], and incorporation of dielectric vias [14].

Directional CP antennas are useful for certain applications, such as satellite communication [15], indoor base stations [16], fixed wireless access systems [17], and ISM-band IoT applications [18]. However, CP antennas radiating at a specific angle often suffer from narrow axial ratio (AR) bandwidths, e.g., [19, 20]. The flexibility of DRs can help solve this issue. By adjusting the shape and materials of a DR, a wider AR bandwidth can be achieved using a simple, low-loss feeding method. For example, a DRA design in [21] obtains a 43.7% bandwidth with a broadside radiation pattern. This superiority of DRA has not been used in tilted-angle antenna design.

In this paper, we present a directional CP DRA design method allowing a specified radiation angle with a considerable bandwidth. For demonstration, a compact, single-feed 3D-printed CP DRA with a main beam tilted at 30° is designed at a 5G frequency of 5.8 GHz. The DRA is segmented into 7 concentric rings. Each ring has 16 angular sectors, forming a total of 112 dielectric blocks. To assist our design, the particle swarm optimization (PSO) is used. As an evolutionary algorithm, PSO is a popular method in facilitating antenna designs [22–24]. As concluded in [23], PSO is recognized for its fast convergence and minimal parameter tuning requirements.

Using the PSO method, an irregular structure is synthesized by optimizing the height and dielectric constant of each block. To validate the design, a prototype is fabricated using 3D-printing technology. Measurements of the prototype confirm that its main beam is directed at 27°, closely matching the desired angle. The fabricated antenna exhibits a low profile ($0.2\lambda_0$ at 5.8 GHz), a wide AR bandwidth of 15.52% (5.3 GHz–6.2 GHz), stable gain performance, a peak gain of 5.87 dBi, and a peak total efficiency of 96%.

* Corresponding author: Kwok Wa Leung (eekleung@cityu.edu.hk).

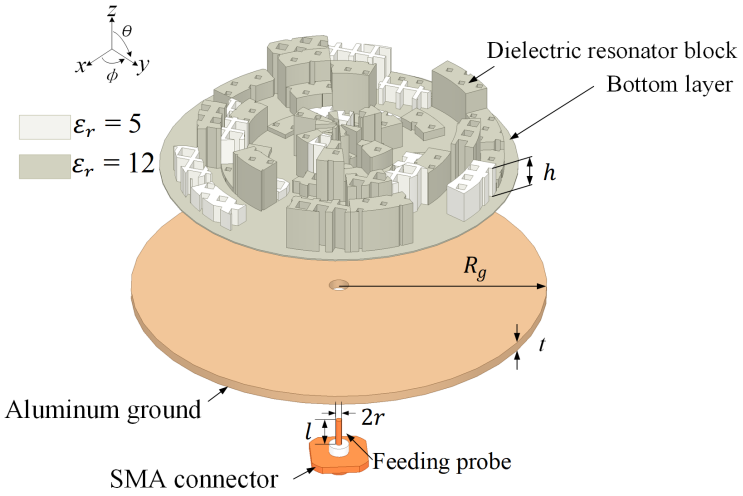

FIGURE 1. Configuration of the 3D-printed irregular DRA.

2. ANTENNA DESIGN

2.1. Antenna Configuration

Figure 1 shows the configuration of our irregular 3D-printed CP DRA obtained via the PSO algorithm. As can be observed from this figure, the structure consists of multiple DR blocks, each with different effective dielectric constants and heights. In this design, two materials with dielectric constants of 5 and 12 are utilized. Table 1 shows the physical properties of these two 3D-printing materials. With reference to the table, the two materials have an ε_r tolerance of ± 0.1 and ± 0.5, with loss tangent of 0.0036 and 0.0029, respectively. Different effective dielectric constants are obtained through varying air-filling ratios of the materials [25]. The DRA is excited by a central coaxial probe with a length of l. It is mounted on a circular aluminum ground plane.

We simulated the antenna using the dielectric properties in Table 1, assuming that they are frequency-stable. To evaluate the effect of potential deviations on the dielectric constant, we performed a sensitivity analysis by considering three cases: (i) normal case ($\varepsilon_{r1} = 5, \varepsilon_{r2} = 12$), (ii) extremely low case ($\varepsilon_{r1} = 4.9$, $\varepsilon_{r2} = 11.5$), and (iii) extremely high case ($\varepsilon_{r1} = 5.1$, $\varepsilon_{r2} = 12.5$). In all these cases, ε_{r1} and ε_{r2} are the dielectric constants of our two 3D-printing materials.

TABLE 1. Physical properties of two 3D-printing materials.

ε_r	Tolerance of ε_r	Loss tangent
5	± 0.1	0.0036
12	± 0.5	0.0029

As shown in Figs. 2(a)–2(c), the dielectric constant variation leads to a slight frequency shift ($\leq$ 0.1 GHz). More importantly, the radiation patterns shown in Fig. 2(d) remain stable across all cases. It should be mentioned that extreme cases are rare. The material tolerances and fabrication errors are not critical in the antenna design.

2.2. Antenna Optimization

The antenna originates from a large solid dielectric cylinder, as shown in Fig. 3. The dielectric cylinder is divided into 7 concentric layers, with each layer further partitioned into 16 angular sections, resulting in a total of $7 \times 16 = 112$ DR blocks. This segmentation scheme ensures the freedom and flexibility of the design while maintaining the optimization efficiency. To obtain the desired main beam, the antenna is optimized by adjusting the height (h) and dielectric constant (ε_r) of each DR block. In doing the optimization, h is an integer ranging from 0 mm to 10 mm, whereas ε_r is selected from (1, 2.5, 4, 5.5, 7, 8.5, 10), i.e., from 1 to 10 with an interval of 1.5.

Since there are as many as 112 dielectric blocks, manual adjustment is impractical. Therefore, a PSO algorithm is deployed. Fig. 4 shows the antenna design process using PSO. It begins with the initialization of block height h and dielectric constant ε_r within predefined constraints, i.e., $h \in \{0, 1, 2, \ldots 10\,\text{mm}\}$ and $\varepsilon_r \in \{1, 2.5, 4, 5.5, 7, 8.5, 10\}$. The PSO used 10 particles with a maximum of 100 iterations. Its inertia weight ω, cognitive coefficient c_1, and social coefficient c_2 are set as 0.8, 0.1, and 0.5, respectively. Each set of generated antenna parameters was simulated in High Frequency Structure Simulator (HFSS). Three performance metrics, reflection coefficient (S_{11}), radiation pattern (RP), and AR, are evaluated by their respective cost functions — $cost_{S_{11}}$, $cost_{RP}$, and $cost_{AR}$. The total cost is formulated as follows:

$$cost = cost_{S_{11}} + 0.5\, cost_{RP} + cost_{AR} \tag{1}$$

where

$$cost_{S_{11}} = \left\| \max\left(0, S_{11}^{in\text{-}band} - (-10)\right) \right\|_2 \tag{2}$$

$$\begin{aligned} cost_{RP} = {} & \left| \hat{\theta}_0 - \theta_0 \right| \\ & + \left\| \max\left(0, G_{co}(\theta,\varphi) - G_{upper}(\theta,\varphi)\right) \right\|_1 \\ & + \left\| \max\left(0, G_{lower}(\theta,\varphi) - G_{co}(\theta,\varphi)\right) \right\|_1 \\ & + \max\left(0, 15 - \min\left(G_{co}(\theta,\varphi) - G_{cr}(\theta,\varphi)\right)\right) \end{aligned} \tag{3}$$

$$cost_{AR} = \left\| \max\left(0, AR^{in\text{-}band} - 3\right) \right\|_2 \tag{4}$$

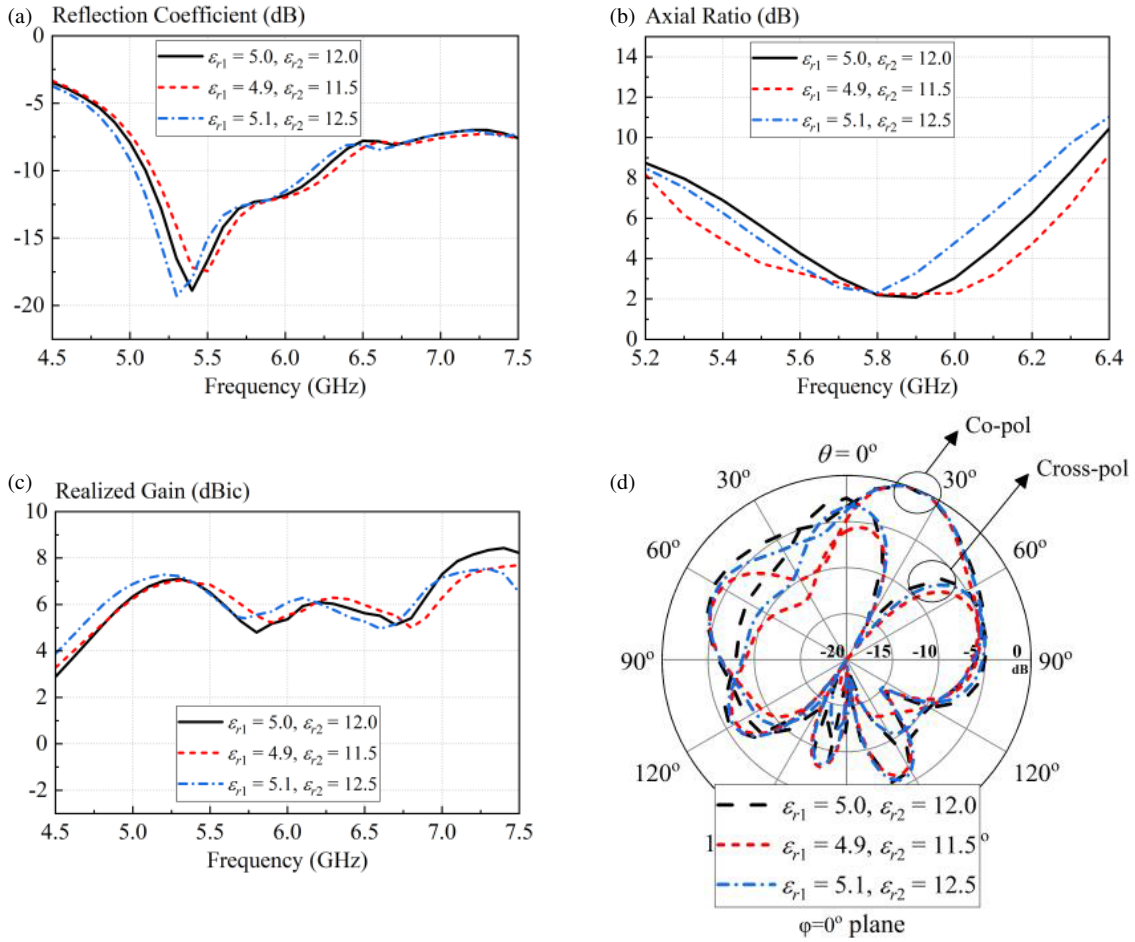

FIGURE 2. Comparison between the normal case and the two extreme cases. (a) Reflection coefficient. (b) AR. (c) Realized gain. (d) Radiation pattern.

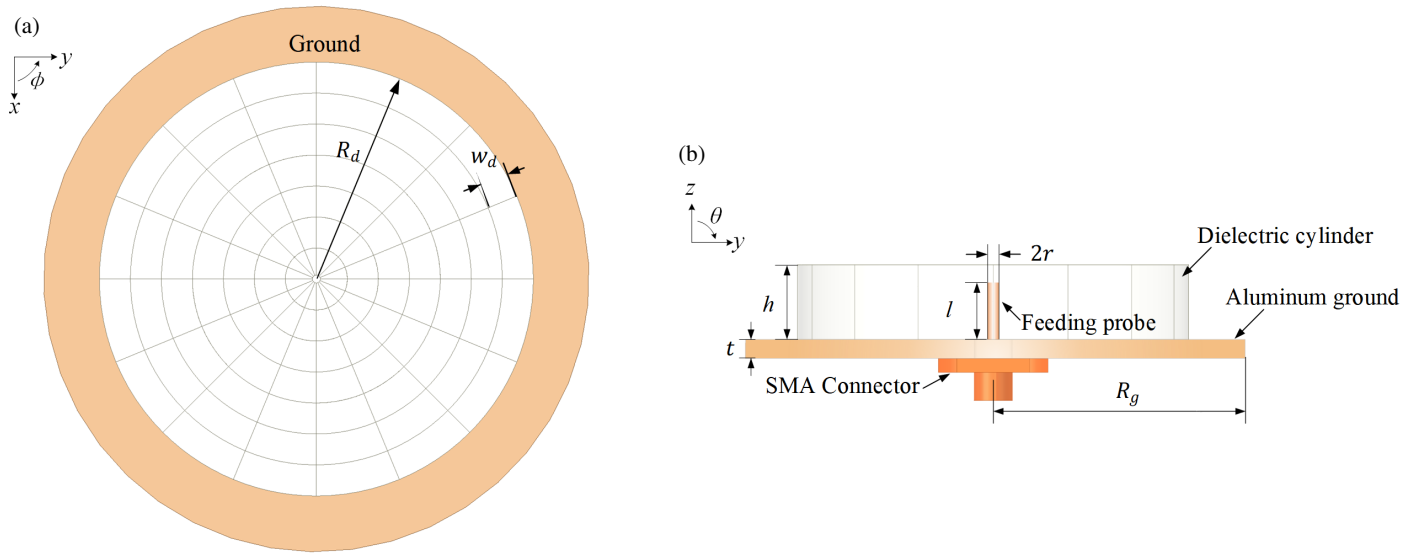

FIGURE 3. Structure of the initial cylindrical DRA. (a) Top view: $R_d = 35\,\text{mm}$, $w_d = 5\,\text{mm}$ ($d = 1, 2, \ldots, 7$). (b) Front view: $l = 6.5\,\text{mm}$, $h \in \{0, 1, 2, \ldots, 10\,\text{mm}\}$, $2r = 1.27\,\text{mm}$, $t = 2\,\text{mm}$, $R_g = 44\,\text{mm}$.

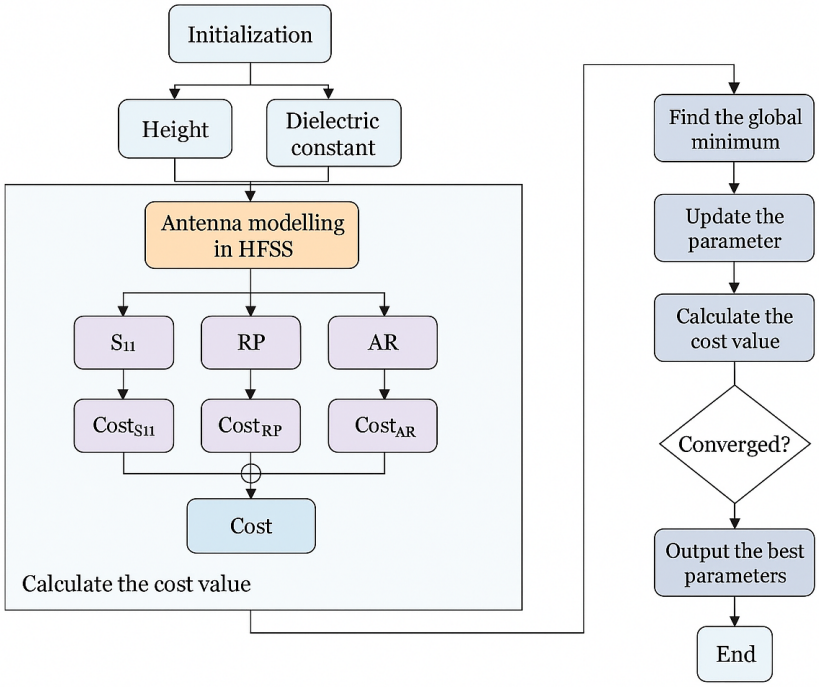

FIGURE 4. Design process.

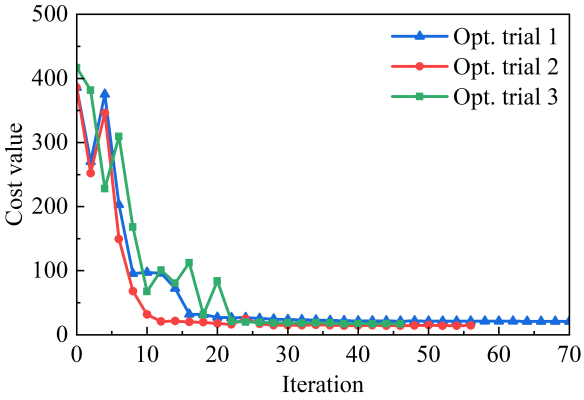

FIGURE 5. Convergence results of three optimization trials.

The weighting ratio in (1) was determined experimentally to balance the different scales of each metric. In (2), the term $S_{11}^{in\text{-}band}$ denotes the reflection coefficient within the targeted frequency band. Since the desired operating frequency is 5.8 GHz, the targeted frequency band is extended from 5.4 to 6.2 GHz. For (3), $\hat{\theta}_0$ and θ_0 denote the current and objective main-beam angles, respectively, whereas G_{co} and G_{cr} are the co- and cross-polar radiation patterns at 5.8 GHz, respectively. The main-beam angle θ_{mb} covers $[\theta_0 - 30°, \theta_0 + 30°]$, and the back-lobe angle θ_{bl} covers $[\theta_0 + 150°, \theta_0 + 210°]$. Finally, $AR^{in\text{-}band}$ in (4) refers to the AR values across the targeted frequency band. Theoretically, a smaller angular resolution, which controls the elevation angle step size, can improve optimization accuracy at the cost of increasing computation time. Since this study aims to demonstrate the design idea, a large angular resolution of 10° was used to reduce the computation time. As a result, the solution has a tolerance of ±10°. This cost is used to guide the PSO process, which iteratively updates the parameters in search of a global minimum. The process continues until the convergence is achieved, where the optimal antenna configuration is obtained and output.

Three optimization trials with different randomly initialized parameters were conducted to avoid local optima. Fig. 5 shows their convergence results. With reference to the figure, the cost values stabilize at around 12 in all cases. It desirably indicates consistent optimization performance and robustness of the method. The best antenna structure was chosen from these optimized solutions.

Figure 6 shows the optimized solid DRA structure. As illustrated in the figure, both the height and dielectric constant show noticeable variations across the dielectric blocks. Since h is allowed to be 0 mm, some blocks entirely disappear. The various optimized dielectric constants given in the figure are realized using different air-filling ratios as discussed in [25].

3. MEASURED AND SIMULATED RESULTS

The prototype was printed using a Creator Pro 2 3D-printer. For ease of assembly, a thin dielectric layer having a thickness of 0.3 mm and a radius of 38 mm was printed beneath the DRA. It took approximately 3 hours 50 minutes to print the prototype in Fig. 7.

Figure 8 shows the simulated and measured radiation patterns of the prototype at 5.8 GHz. Fig. 8(a) shows the simulated 3D radiation pattern, whereas Fig. 8(b) shows the simulated and measured radiation patterns in the x-z plane. Reasonable agreement between the measured and simulated results is observed. With reference to the figure, the measured radiation pattern shows reduced leakage in the broadside direction

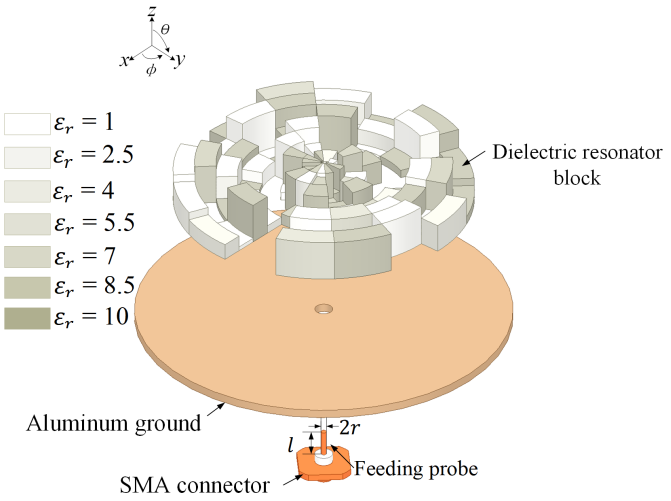

FIGURE 6. Structure of the optimized solid DRA.

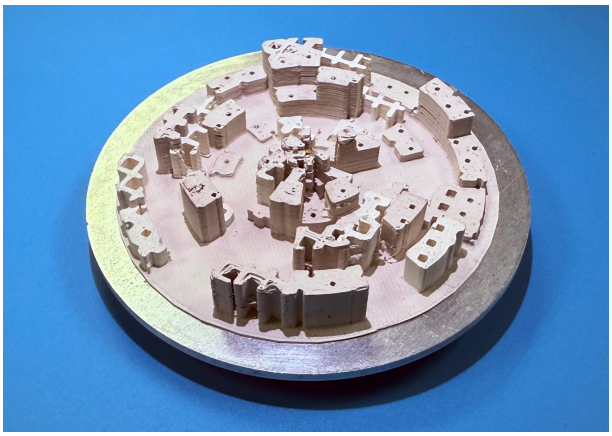

FIGURE 7. 3D-printed prototype of the DRA.

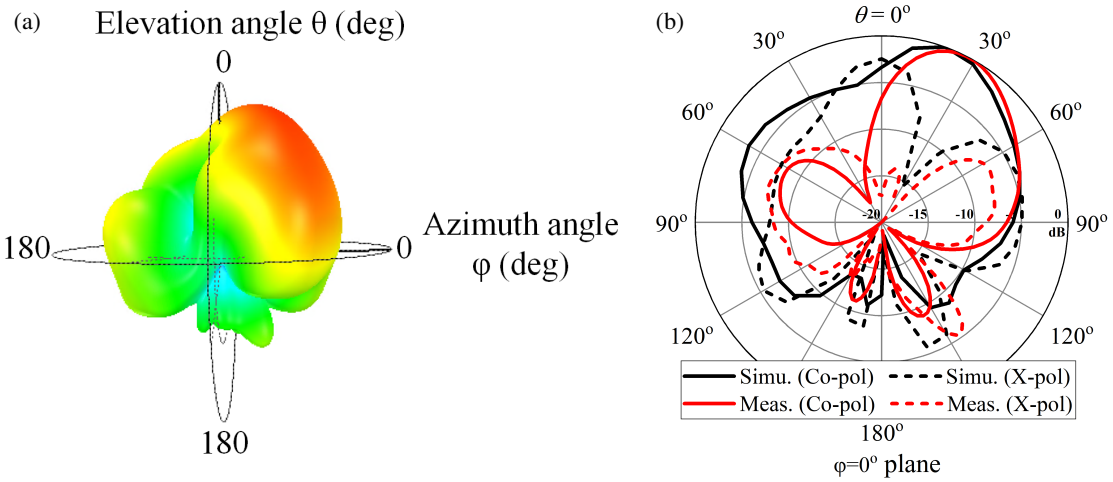

FIGURE 8. Radiation pattern at 5.8 GHz. (a) Simulated 3D radiation pattern; (b) Simulated and measured radiation pattern in the x-z plane (azimuth angle $\varphi = 0^0$ plane).

as compared with the simulation. This difference may result from slightly increased asymmetries due to fabrication errors and additional loss in the feeding probe. While this reduces the cross-polarization, it also leads to a narrower beamwidth than the simulation. As shown in the figure, the measured main-beam direction is along 27°, which is close to the designed value of 30°. This angle deviation is within the tolerance of ±10°. At the main beam angle, the measured co-polar field is stronger than the cross-polar field by 18 dB, showing that the DRA has a good polarization purity.

Figure 9 shows the E-field distribution of the designed DRA at 5.8 GHz. To explain the CP mechanism, the E-field is displayed at two key phases: 0° and 90°. At these two phases, the strongest E-field locations are spatially shifted, showing a 90° phase difference. This phase shift and spatial rotation of the E-field generate a CP wave and enable the beam to tilt in the desired direction.

Figure 10 shows the simulated and measured reflection coefficients of the DRA prototype. It was measured using an N5230A vector network analyzer. With reference to the figure, the measured result agrees reasonably well with the simulated one, validating the research idea. The antenna exhibits a good impedance match across the frequency band of concern. It can be found from the figure that the measured −10 dB bandwidth is 37.2%. It is much wider than that of the simulated counterpart due to fabrication errors and experimental imperfections. For example, loss in the connectors and coaxial cable can decrease the overall Q-factor and hence, increase the bandwidth. Also, the fabricated dimension error has inevitably affected the impedance matching level.

Far-field radiation characteristics were measured using a Satimo StarLab system. Fig. 11 shows the simulated and measured ARs. With reference to this figure, the simulated and measured ARs are 2.18 dB and 1.51 dB at 5.8 GHz, respectively. It can be observed from the figure that the measured AR bandwidth (15.52%) is much wider than the simulated counterpart, which is consistent with impedance bandwidth results.

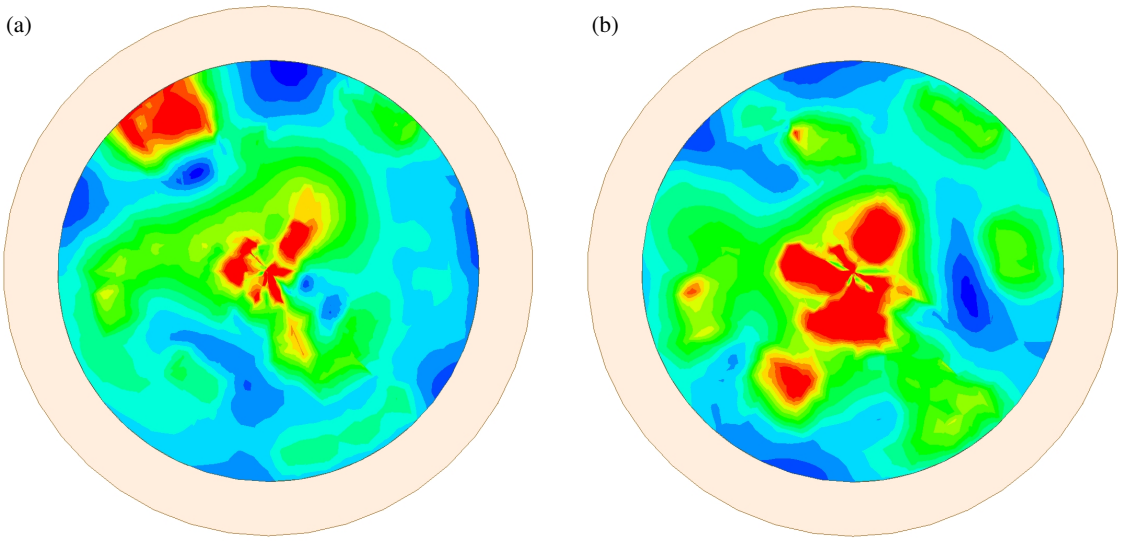

FIGURE 9. E-field in the designed DRA at 5.8 GHz. (a) Phase = 0°. (b) Phase = 90°.

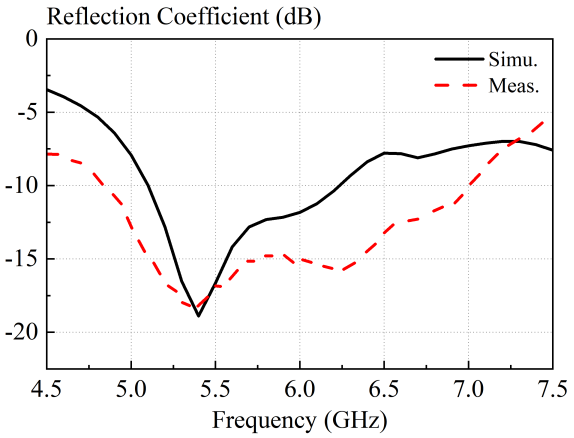

FIGURE 10. Simulated and measured reflection coefficients of the DRA.

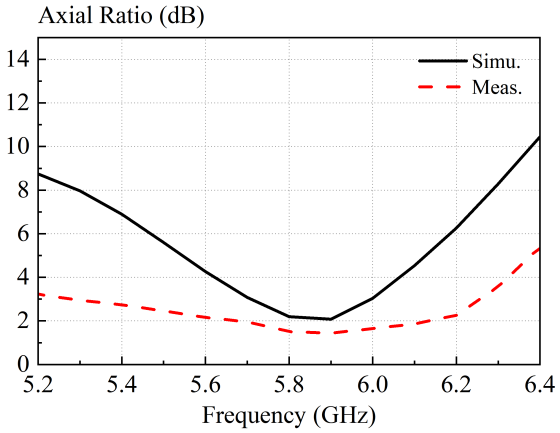

FIGURE 11. Simulated and measured ARs of the DRA.

Figure 12 shows the simulated and measured antenna gains. As seen in the figure, the simulated and measured results are in reasonable agreement. The measured gain is slightly higher than the simulated values from 5.8 to 6.0 GHz. This is not surprising because the measured reflection coefficient in Fig. 10 indicates a better impedance match in this frequency range. Across the overlapping passband of impedance and AR (5.3–6.2 GHz), the measured realized gain varies between 5.08 and 6.3 dBic.

Figure 13 shows the measured total antenna efficiency. As can be observed from the figure, the antenna has an average measured result of 91.6% over the overlapping passband (5.3–6.2 GHz), with a peak total antenna efficiency reaching up to 96%.

To further illustrate the superiority of our design, Table 2 compares our antenna and the state-of-the-art tilted-beam antennas. Our antenna is the only DRA among the tilted-angle antennas in the table. Compared to the existing tilted-beam CP antennas, this work achieves the widest overlapped bandwidth (15.52%) of AR and impedance at a tilting angle of 30°, while maintaining a compact, single-feed structure. The same design method can produce antennas with different radiation directions. Our antenna maintains very high total efficiency (91.6% on average and 96% at peak), indicating minimal optimization loss. These advantages make it suitable for broadband CP applications requiring simple hardware and wide coverage, such as vehicular ISM-band communications and fixed wireless access terminals.

4. STUDY ON THE TILTED ANGLE LIMITATION

Theoretically, antennas with different tilting angles can be designed by optimizing the height and dielectric constant of the 112 DR blocks. To investigate the structure limitation, a DRA with a large tilting angle of 90° was optimized. Fig. 14 shows the results in 60 rounds of PSO iterations. Fig. 14(a) presents the solid structure of the designed 90° DRA. Fig. 14(b) shows the radiation pattern in the x-z plane. With reference to this figure, the main beam is tilted at 70°, which deviates 20° from the intended 90°. This represents the best achievable result. In

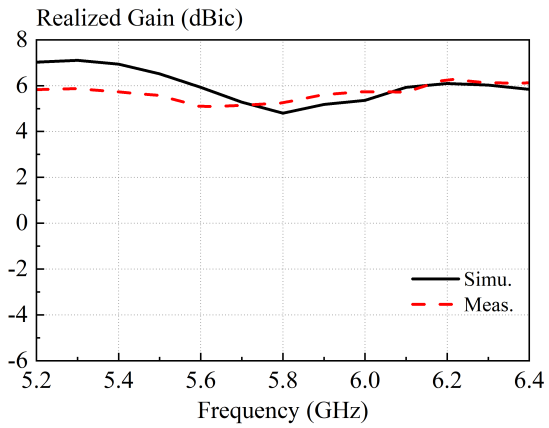

FIGURE 12. Simulated and measured gains of the DRA.

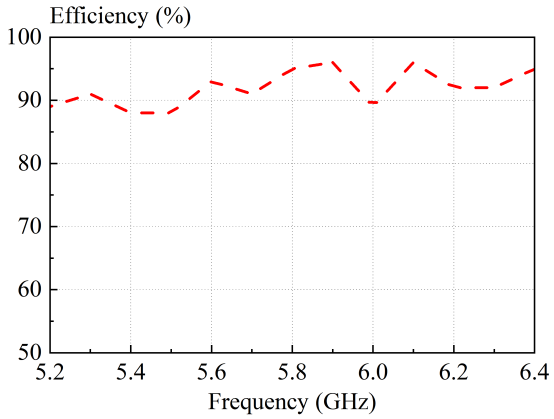

FIGURE 13. Measured total antenna efficiency of the 3D-printed DRA.

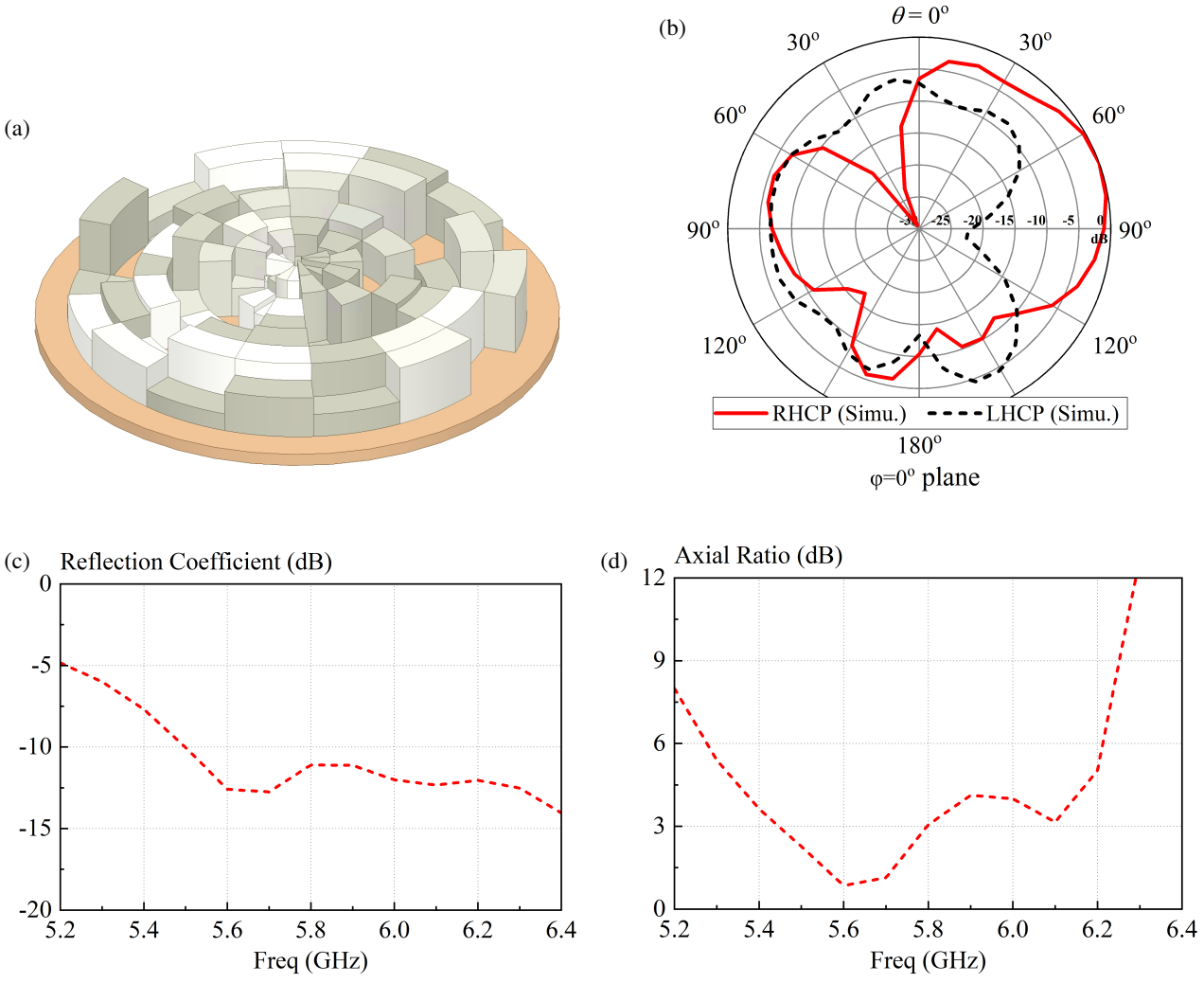

FIGURE 14. Design of the 90° tilted-beam DRA. (a) Antenna structure. (b) Simulated radiation pattern at the designed plane at 5.8 GHz. (c) Simulated reflection coefficient. (d) Simulated AR.

other words, a 90° main-beam angle is practically unrealizable. The limitation arises from two factors. First, the ground plane confines radiation to the upper hemisphere ($z > 0$). Second, the block segmentation (7×16) and the availability of dielectric constants ($\varepsilon_r = 1$–10) restrict the aperture field synthesis. The 3D-printed dielectric-block structure acts as a radiating aperture. Its main beam angle θ_0 is related to the progressive phase

TABLE 2. Comparison between our designed antenna and other works.

Ref.	Overlap bandwidth	Design angle	Peak gain (dBic)	Efficiency	Dimension	Single-feed
[15]	6.19%	30°	8.0	81%	$0.98\lambda_0 \times 1.44\lambda_0 \times 0.38\lambda_0$	Yes
[26]	12.0%	25°	6.97	91%	$R0.22\lambda_0 \times 0.07\lambda_0$	Yes
[27]	7.5%	46°	10.5	∼ 97%	$3.65\lambda_0 \times 2.11\lambda_0 \times 0.62\lambda_0$	Yes
[28]	10.0%	∼ 30°	8.1	83%	$0.82\lambda_0 \times 1.225\lambda_0 \times 0.034\lambda_0$	No
[18]	11.57%	30°	8.73	96%	$0.73\lambda_0 \times 1.19\lambda_0 \times 0.07\lambda_0$	Yes
This work	15.52%	30°	6.3	91.6% (96%)	$R0.85\lambda_0 \times 0.23\lambda_0$	Yes

shift $\Delta\varphi$ across the effective aperture, expressed as

$$k_0 sin(\theta_0) = \Delta\varphi/d \tag{5}$$

where $k_0 = 2\pi/\lambda$ is the free-space wavenumber, and d is the effective spacing between adjacent radiating elements (i.e., the dielectric blocks). To have tilt angles close to 90°, a large progressive phase shift $\Delta\varphi$ will be required. However, due to the constraint of size and material, this configuration has a practical limit of about 70°. Figs. 14(c) and 14(d) show the S_{11} and AR, respectively. As can be observed from the figure, the 90° antenna meets the impedance matching and AR requirements at 5.8 GHz although it has a limited bandwidth.

5. CONCLUSION

In this paper, a directional CP DRA allowing a specified radiation angle design has been designed using the PSO method. To demonstrate the idea, a single-feed, low-profile prototype with a main beam angle at 30° has been 3D-printed. The structure consists of 112 dielectric blocks, each optimized for height and dielectric constant to form an irregular configuration that enables directional CP radiation.

Measured results have shown a −10 dB impedance bandwidth of 37.2%, a 3-dB AR bandwidth of 15.52%, a peak gain of 5.87 dBic, and peak total efficiency of 96%. The measured main beam is directed at 27°, closely matching the target angle. These measured results have successfully verified the effectiveness of the PSO-based optimization and the feasibility of the 3D-printed implementation.

Compared with other reported CP antennas with tilted beams, this work achieves a wider AR bandwidth while maintaining a compact single-feed structure. The proposed approach is versatile, allowing future extensions to other beam tilting angles or multi-beam designs. With its simplified feeding mechanism, high efficiency, and robust directionality, this antenna is well-suited for practical applications such as vehicular ISM-band communication, indoor base stations, and fixed wireless access systems, where beam tilting and circular polarization are required.

ACKNOWLEDGEMENT

This work was supported by the International Cooperation Research Program of Guangzhou Development District under Grant 2023GH06. The authors would like to thank the reviewers for their useful comments.

REFERENCES

[1] Long, S., M. McAllister, and L. Shen, "The resonant cylindrical dielectric cavity antenna," *IEEE Transactions on Antennas and Propagation*, Vol. 31, No. 3, 406–412, 1983.

[2] Petosa, A. and A. Ittipiboon, "Dielectric resonator antennas: A historical review and the current state of the art," *IEEE Antennas and Propagation Magazine*, Vol. 52, No. 5, 91–116, 2010.

[3] Petosa, A., *Dielectric Resonator Antenna Handbook*, Artech, 2007.

[4] Luk, K. M. and K. W. Leung, *Dielectric Resonator Antennas*, Research Studies Press, 2003.

[5] Leung, K. W., E. H. Lim, and X. S. Fang, "Dielectric resonator antennas: From the basic to the aesthetic," *Proceedings of The IEEE*, Vol. 100, No. 7, 2181–2193, 2012.

[6] Wang, K. X. and H. Wong, "A circularly polarized antenna by using rotated-stair dielectric resonator," *IEEE Antennas and Wireless Propagation Letters*, Vol. 14, 787–790, 2014.

[7] Pan, Y. and K. W. Leung, "Wideband circularly polarized trapezoidal dielectric resonator antenna," *IEEE Antennas and Wireless Propagation Letters*, Vol. 9, 588–591, 2010.

[8] Zou, M., J. Pan, and Z. Nie, "A wideband circularly polarized rectangular dielectric resonator antenna excited by an archimedean spiral slot," *IEEE Antennas and Wireless Propagation Letters*, Vol. 14, 446–449, 2015.

[9] Varshney, G., V. S. Pandey, R. S. Yaduvanshi, and L. Kumar, "Wide band circularly polarized dielectric resonator antenna with stair-shaped slot excitation," *IEEE Transactions on Antennas and Propagation*, Vol. 65, No. 3, 1380–1383, 2017.

[10] Lu, L., Y.-C. Jiao, H. Zhang, R. Wang, and T. Li, "Wideband circularly polarized antenna with stair-shaped dielectric resonator and open-ended slot ground," *IEEE Antennas and Wireless Propagation Letters*, Vol. 15, 1755–1758, 2016.

[11] Pan, Y. M., W. J. Yang, S. Y. Zheng, and P. F. Hu, "Design of wideband circularly polarized antenna using coupled rotated vertical metallic plates," *IEEE Transactions on Antennas and Propagation*, Vol. 66, No. 1, 42–49, 2018.

[12] Yang, M., Y. Pan, and W. Yang, "A singly fed wideband circularly polarized dielectric resonator antenna," *IEEE Antennas and Wireless Propagation Letters*, Vol. 17, No. 8, 1515–1518, 2018.

[13] Fakhte, S., H. Oraizi, R. Karimian, and R. Fakhte, "A new wideband circularly polarized stair-shaped dielectric resonator antenna," *IEEE Transactions on Antennas and Propagation*, Vol. 63, No. 4, 1828–1832, 2015.

[14] Tong, C., H. I. Kremer, N. Yang, and K. W. Leung, "Compact wideband circularly polarized dielectric resonator antenna with dielectric vias," *IEEE Antennas and Wireless Propagation Letters*, Vol. 21, No. 6, 1100–1104, 2022.

[15] Zhang, W.-H., W.-J. Lu, and K.-W. Tam, "Circularly polarized complementary antenna with tilted beam based on orthogo-

nal dipoles," *IEEE Antennas and Wireless Propagation Letters*, Vol. 17, No. 8, 1406–1410, 2018.

[16] Chen, Z., Q. Liu, B. Sanz-Izquierdo, H. Liu, J. Yu, and X. Chen, "A wideband circular-polarized beam steering dielectric resonator antenna using gravitational ball lens," *IEEE Transactions on Antennas and Propagation*, Vol. 69, No. 5, 2963–2968, 2021.

[17] Zhang, M., S. Matsueda, J. Hirokawa, and M. Ando, "Realization of a beam-tilted circularly polarized corporate-fed waveguide slot array in the 60 GHz band," *IEEE Transactions on Antennas and Propagation*, Vol. 69, No. 12, 8967–8972, 2021.

[18] Li, M., Z. Sun, M.-C. Tang, and L. Zhu, "Broadband circularly polarized microstrip antenna with customized tilted beam based on index-modulated folded split ring resonator," *IEEE Transactions on Antennas and Propagation*, Vol. 72, No. 3, 2831–2836, 2024.

[19] Ijiguchi, T., D. Kanemoto, K. Yoshitomi, K. Yoshida, A. Ishikawa, S. Fukagawa, N. Kodama, A. Tahira, and H. Kanaya, "Circularly polarized one-sided directional slot antenna with reflector metal for 5.8-GHz DSRC operations," *IEEE Antennas and Wireless Propagation Letters*, Vol. 13, 778–781, 2014.

[20] Ye, M., X.-R. Li, and Q.-X. Chu, "Single-layer circularly polarized antenna with fan-beam endfire radiation," *IEEE Antennas and Wireless Propagation Letters*, Vol. 16, 20–23, 2017.

[21] Yadav, S. K., A. Kaur, and R. Khanna, "Broadband circularly polarized dielectric resonator antenna for UWB applications," *Sadhana*, Vol. 47, No. 2, 48, Springer, 2022.

[22] Panduro, M. A. and C. A. Brizuela, "A comparative analysis of the performance of GA, PSO and DE for circular antenna arrays," in *2009 IEEE Antennas and Propagation Society International Symposium*, 1–4, North Charleston, SC, USA, Jun. 2009.

[23] Rahmat-Samii, Y. and D. H. Werner, "A comprehensive review of optimization techniques in electromagnetics: Past, present, and future," *IEEE Transactions on Antennas and Propagation*, IEEE, 2025.

[24] Akila, M., P. Anusha, M. Sindhu, and K. T. Selvan, "Examination of PSO, GA-PSO and ACO algorithms for the design optimization of printed antennas," in *2017 IEEE Applied Electromagnetics Conference (AEMC)*, 1–2, Aurangabad, India, Dec. 2017.

[25] Xia, Z.-X., K. W. Leung, and K. Lu, "3-d-printed wideband multi-ring dielectric resonator antenna," *IEEE Antennas and Wireless Propagation Letters*, Vol. 18, No. 10, 2110–2114, 2019.

[26] Yu, J., W.-J. Lu, Y. Cheng, and L. Zhu, "Tilted circularly polarized beam microstrip antenna with miniaturized circular sector patch under wideband dual-mode resonance," *IEEE Transactions on Antennas and Propagation*, Vol. 68, No. 9, 6580–6590, IEEE, 2020.

[27] Rao, P. H., G. Praveen, C. Anukumar, G. Kailash, and Y. K. Verma, "Circularly polarised printed tilted beam antenna," *IET Microwaves, Antennas & Propagation*, Vol. 13, No. 4, 510–518, 2019.

[28] Khidre, A., F. Yang, and A. Z. Elsherbeni, "Circularly polarized beam-scanning microstrip antenna using a reconfigurable parasitic patch of tunable electrical size," *IEEE Transactions on Antennas and Propagation*, Vol. 63, No. 7, 2858–2866, 2015.